Microstructure of dense colloid–polymer suspensions and gels

2003 J. Phys.: Condens. Matter 15 4751

(http://iopscience.iop.org/0953-8984/15/27/308)

INSTITUTE OF PHYSICS PUBLISHING JOURNAL OF PHYSICS: CONDENSED MATTER

J. Phys.: Condens. Matter **15** (2003) 4751–4778 PII: S0953-8984(03)59618-7

Microstructure of dense colloid–polymer suspensions and gels

S A Shah, Y-L Chen, S Ramakrishnan, K S Schweizer[1] and C F Zukoski[1]

Departments of Chemical and Biomolecular Engineering, Materials Science and Engineering, and Materials Research Laboratory, University of Illinois, Urbana, IL 61801, USA

E-mail: kschweiz@uiuc.edu and czukoski@uiuc.edu

Received 13 February 2003, in final form 12 May 2003
Published 27 June 2003
Online at stacks.iop.org/JPhysCM/15/4751

Abstract

A systematic experimental study of polymer-induced changes of the collective structure of model hard-sphere nanocolloids in the fluid and gel states has been carried out using ultra-small-angle x-ray scattering. The focus is on small, non-adsorbing polymer depletants where a direct transition from the homogeneous fluid phase to a nonequilibrium gel state occurs with increasing polymer additions. As the polymer concentration is increased in the homogeneous fluid phase, the low angle concentration fluctuations monotonically increase, the characteristic interparticle separation decreases and tends to saturate, and the intensity of the cage order peak varies in a non-monotonic manner. These equilibrium structural changes depend in a systematic fashion on colloid volume fraction and polymer–colloid size asymmetry, and are in near quantitative agreement with the parameter-free polymer reference interaction site model theory calculations. By combining the accurate equilibrium theory with experimental observations, the loss of ergodicity and nonequilibrium structure formation in the gel state can be deduced. Abrupt departures between theory and experiment on the ∼2–3 particle diameter and greater length scales are observed as the gel boundary is traversed. The liquid-like local cage structure is arrested. Intermediate scale fluctuations are suppressed suggesting the formation of small, compact clusters. Large amplitude, Porod-like fluctuations emerge on large length scales due to quenched heterogeneities which are analysed using a random two-phase composite model. By combining the results of all the scattering experiments and theoretical calculations a qualitative real space picture of the gel microstructure is constructed, and its mechanical consequences are qualitatively discussed.

[1] Authors to whom any correspondence should be addressed.

0953-8984/03/274751+28$30.00

1. Introduction

Colloidal and nanoparticle suspensions which undergo a fluid-to-gel transition constitute a class of materials of enormous technological significance [1]. A gel is a nonergodic, space-filling soft solid where long range diffusive motion is arrested. Controlling the gel microstructure and mechanical properties are the basis of much of the interest in these materials. Recent studies demonstrate that gels can form from the homogeneous fluid phase with increasing strength of interparticle attraction when the range of the attraction is less than about a tenth of a particle radius, R [2–5]. The suspension flow properties change from liquid-like to solid-like in that relaxation times grow to be longer than the experimental observation time and the material displays a dynamic yield stress [6–9]. The thermodynamic properties near this ergodic/nonergodic transition, and changes in collective structure through the gelation transition, are poorly characterized. This lack of understanding limits technological applications where tuning material properties is important. Of particular interest in this study is the effect of short-range attractions on the suspension microstructure as the gel boundary is crossed.

Depletion attractions between hard-sphere particles resulting from the addition of nonadsorbing polymers provide a model system for systematically changing the strength and range of the interparticle attractions in a relatively gentle and controllable manner [2, 10–15]. When the polymer radius of gyration, R_g, is much smaller than the particle radius, R, the range of the induced attraction is small. At polymer concentrations, c_p, well below where polymer coils begin to overlap, the suspensions gel. This nonequilibrium transition can pre-empt the equilibrium fluid–fluid and fluid–crystal phase transitions, or occur in a two-phase coexistence region [2–5]. Gelation bears some similarities to the hard-sphere glass transition which occurs at a particle volume fraction of $\phi_c \sim 0.58$ [16]. Both kinetic vitrification and gelation are characterized by a separation of timescales as observed in the autocorrelation function of particle concentration fluctuations measured by dynamic light scattering. At the transition, the slowest relaxation time effectively diverges, demonstrating the loss of ergodicity, and marking the point where the suspension falls out of equilibrium [16].

Vitrification and gelation also differ in several fundamental aspects. The hard-sphere glass transition is induced by increasing the suspension volume fraction, resulting in a repulsive force driven jamming and localization of particles on the cage length scale [16–18]. Gelation occurs over a wide range of volume fractions and is induced by increasing the strength of interparticle attractions, resulting in the formation of effectively permanent 'bonds' and connectivity percolation [2]. Recent studies show attractions induced through the addition of small non-adsorbing polymers can result in a 'melting' of the hard-sphere glass corresponding to a shift of the vitrification volume fraction to higher values [14, 19–23]. The structural signature for this effect is a decrease of the magnitude of the first wide-angle 'cage order' peak of the colloidal structure factor. Upon further increase of polymer concentration, depletion attractions drive a gelation transition with particles localized on a length scale controlled by the spatial range of the depletion attraction [2, 19–23].

A few small-angle scattering experiments which probe the structural consequences of attractions have been reported in the fluid state. Ye *et al* [24] employed small-angle neutron scattering (SANS) to characterize the long-wavelength structure of relatively low volume fraction nanoparticle–polymer suspensions under conditions where $R_g/R \sim 2$. They compared their data with predictions based on a simplified effective one-component depletion potential [15]. The comparison required numerous fitting parameters to account for the effects of size polydispersity, soft particle interactions, the relatively large polymer-to-particle asymmetry ratio and non-dilute polymer concentrations, but provided qualitative evidence for the effects of increasing polymer concentration on the suspension microstructure.

Recent light scattering studies of the local and long wavelength structure of colloid–polymer (CP) mixtures have also been performed [25]. Excellent quantitative agreement with the no-adjustable parameter structure factor predictions of the polymer reference interaction site model (PRISM) theory has been demonstrated [26]. In contrast to classical models [13, 27] which ignore polymer conformational degrees of freedom and polymer–polymer interactions, PRISM theory correctly predicts changes in the equilibrium fluid–fluid phase separation boundaries of CP mixtures as a function of the solvent quality, range of attraction and particle volume fraction [3–5, 26]. Limited scattering studies have been reported for the structure of CP gels [2, 21, 25, 28].

Real space images of depletion flocculated gels have been recently obtained [29] for dilute particle suspensions ($\phi_c \leqslant 0.1$). Under the conditions studied ($R_g/R \leqslant 0.27$), kinetic gelation appears to be in an intermediate regime between the limiting cases of diffusion- and reaction-limited cluster aggregation, with a time-invariant mass fractal exponent of $d_f \sim 2$. Samples deep inside the gel region of the phase diagram had fewer bonds per particle, forming more open chain-like clusters. Increasing the polymer or particle concentrations monotonically reduced the number of bonds per particle. This type of increased structural heterogeneity has also been reported for dense thermoreversible colloidal gels ($0.26 \leqslant \phi_c \leqslant 0.5$) where the adhesive contact of sticky spheres leads to clusters and interstitial voids. At the gelation transition, long-range density fluctuations and voids of a broad volume distribution are the dominant structural features of dense colloidal gels [30].

This paper describes measurements of the collective structure factor of dense colloidal suspensions in the fluid and gel states produced by the addition of small non-adsorbing polymer where $0.05 < R_g/R < 0.08$. Pinhole collimated ultra-small-angle x-ray scattering (USAXS) is employed. As the polymer concentration is increased at fixed ϕ_c, excellent quantitative agreement is demonstrated in the fluid phase with the parameter-free predictions of PRISM theory. Above the polymer concentration where gels are produced, the comparisons are poor, indicating the suspensions have fallen out of equilibrium. Upon gelation, the local cage structure is frozen, intermediate scale fluctuations are suppressed and large small wavevector fluctuations emerge due to heterogeneities or 'clusters'.

The remainder of the paper is structured as follows. In section 2 the experimental system and scattering technique are described. PRISM theory is briefly discussed in section 3. Section 4 presents our experimental measurements of the colloidal structure factors and comparisons with PRISM theory. The dependence of the primary local cage features on polymer concentration, volume fraction and size asymmetry are discussed and compared with theory in section 5. Section 6 discusses the intermediate and long wavelength behaviour. Comparison with equilibrium theory, a fractal cluster model and a random two-phase model of heterogeneous gel structure are presented. Our basic conclusions and physical picture are given in section 7.

2. Experimental details

Silica particles were prepared by the base catalyzed hydrolysis and condensation of tetraethyl orthosilicate according to the method of Stober *et al* [31]. A seeded growth technique developed by Bogush *et al* [32] was used to increase the particle diameter to the desired size. The particles were then rendered hydrophobic via the method of van Helden *et al* [33], where surface silanol groups were esterified with steryl alcohol by boiling at 220 °C for 5 h. The particles were sized using transmission electron microscopy (Philips CM-12 TEM) and dynamic light scattering (DLS-Brookhaven Instruments BI-200 SM goniometer, Lexel Argon-Ion Model 95 laser, $\lambda = 514$ nm).

Particles of radius $R = D/2 = 59 \pm 3$ nm were made to achieve the desired range of polymer/particle size asymmetry ratio $\xi = R_g/R$. The excess steryl alcohol was removed by repeatedly rinsing the particles in chloroform followed by centrifugation and decantation. The silica was dried in a vacuum oven for 24 h to ensure the thorough removal of chloroform. A known mass of dried silica powder was then suspended in a 50:50 mixture of *cis*- and *trans*-decalin purchased from the Sigma-Aldrich Chemical Company, and vigorously stirred to disperse the particles.

In the absence of polymer, the hard sphere suspensions remained stable at room temperature over the time period for which the experiments were conducted. Using the gravimetrically determined density of $\rho_c = 1.9 \pm 0.04$ g cm^{-3}, stock suspensions of known colloid volume fraction (ϕ_c) were prepared. Osmotic compressibility measurements as a function of varying colloid volume fraction have been previously reported [5], and are in excellent agreement with predictions of the Carnahan–Starling equation of state [34]. Small-angle scattering measurements yielded collective structure factors which are in excellent agreement with Percus–Yevick theory [35], and confirm the hard sphere nature of these particles up to $\phi_c \approx 0.45$.

Polystyrene of molecular weights $M_w = 1.32 \times 10^4$ and 2.93×10^4 g mol^{-1} were purchased from the Sigma-Aldrich Chemical Company. The polymer samples have a narrow size distribution with a ratio of the weight average molecular weight to the number average molecular weight less than 1.05. Polymer stock solutions were prepared such that $c_p \geqslant c_p^*$, where c_p is the polymer mass concentration, $c_p^* = 3M_w/4\pi R_g^3 N_A$ is the dilute–semidilute overlap concentration and N_A is Avogadro's number. To determine the appropriate scaling law for the calculation of R_g from molecular weight, the radius of gyration in decalin was measured using static light scattering (using a DAWN DSP-F laser photometer manufactured by Wyatt Technology Corp) for the higher molecular weight polystyrene samples. To within experimental uncertainties, ideal theta solvent behaviour was observed ($R_g \propto M_w^{1/2}$), in accordance with previous studies [36, 37]. This scaling is used to determine the radii of gyration and c_p^* values for the smaller molecular weight polymer used in this study and as previously reported [5].

The effects of increasing the strength of depletion attractions are investigated by varying the polymer concentration (reported in dimensionless form, c_p/c_p^*) at a fixed volume fraction ($\phi_c = 0.40 \pm 0.01$) and two small size asymmetry ratios of $R_g/R = 0.053$ and 0.078. For both systems, gelation occurs directly from the homogeneous fluid phase beyond a critical polymer concentration c_p^{gel}. Experiments at $\phi_c \geqslant 0.4$ were performed to ensure a stable nonergodic gel structure. Fibre optic quasielastic light scattering (FOQELS) measurements show only partial decay of the dynamic correlations and a long time plateau over the timescale of the experiments. Samples with $\phi_c < 0.4$ often collapsed under gravity where dynamic light scattering shows they are ergodic. Based on FOQELS measurements, these samples were ergodic both before and after settling. Hence our 'gel line' at lower ϕ_c is an 'aggregation line' in the nomenclature of Poon *et al* [2, 38]. This is markedly different than the stable, space spanning gels formed at low ϕ_c ($\leqslant 0.05$) in thermoreversible colloidal suspensions, where the strong attractions arise due to adhesion and interdigitation of the thin polymeric coating on the particle surface [39]. Colloid and polymer stock solutions were initially prepared such that suspensions were in the homogeneous fluid phase and the gel boundary was crossed by traversing vertically through the phase diagram. Scattering experiment samples were prepared with equal volumes of polymer stock solution of varying concentrations. These were added to 2 cm^3 of a fixed colloid volume fraction stock solution ($\phi_c^{stock} \sim 0.45$) such that the final colloid volume fraction was the same for all samples. The samples were mixed, ensuring that each had achieved a steady state generated by exposure to a uniform high shear. The effect of increasing volume fraction to

Table 1. Experimental system. Polymer molecular weights, size asymmetry ratio R_g/R (R_g determined from static light scattering measurements and appropriate scaling [36, 37]), colloid volume fraction ϕ_c, reduced polymer concentration and phase (from visual observation) are given. The colloid radius $R = 59 \pm 3$ nm for all samples. The polymer and colloid were suspended in decalin, a near-ideal solvent for polystyrene. The gel boundary for all cases lies within $0.08 \leqslant c_p^{gel}/c_p^* \leqslant 0.1$.

Molecular weight (g mol^{-1}) (R_g (nm))	R_g/R	ϕ_c	c_p/c_p^*	Phase
1.32×10^4	0.053	0.40 ± 0.01	0	Liquid
(3.03)		0.40	0.02	Liquid
		0.40	0.05	Liquid
		0.40	0.1	Gel
		0.40	0.15	Gel
		0.40	0.2	Gel
		0.45 ± 0.01	0	Liquid
		0.45	0.02	Liquid
		0.45	0.04	Liquid
		0.45	0.05	Liquid
		0.45	0.1	Gel
		0.45	0.15	Gel
		0.45	0.2	Gel
2.93×10^4	0.078	0.40 ± 0.01	0.02	Liquid
(4.60)		0.40	0.03	Liquid
		0.40	0.04	Liquid
		0.40	0.05	Liquid
		0.40	0.1	Gel
		0.40	0.15	Gel
		0.40	0.2	Gel

$\phi_c = 0.45$ at $R_g/R = 0.053$ ($M_w = 1.32 \times 10^4$ g mol^{-1}) was also studied. All the sample conditions studied are summarized in table 1.

USAXS experiments were conducted at the UNICAT facility on the 33-ID line, Advanced Photon Source (APS) facility at Argonne National Laboratory. The instrument utilizes a Bonse-Hart camera using Si(111) optics with additional side-reflection stages enabling effective pinhole collimation where unsmeared data are obtained. The beam is 0.4 mm vertical by 1.5 mm horizontal through which 2×10^{13} photons are incident at 10 keV with a wavelength $\lambda = 1.54$ Å. The instrument has a q range of 2×10^{-4}–2×10^{-1} Å^{-1} with a resolution of $\Delta q = 2 \times 10^{-4}$ Å^{-1}. The scattered beam is analysed by a rotating Si(111) channel cut crystal and measured by a photodiode detector. The narrow wavelength resolution ($\Delta\lambda/\lambda = 1.5 \times 10^{-4}$) ensures wavelength smearing effects are insignificant. All samples were loaded in custom-made aluminium cell holders with a 1 mm beam path length, enclosed between two kapton polyimide film windows. Gels were shear melted prior to loading the cells to improve workability. The pre-shearing removed memory of the gel structure associated with initial sample preparation and allowed solvent evaporation to be avoided. The time between sample loading and the start of the x-ray experiments was less than 20 min. Prior studies of gel structure under different rates of shear have shown an enhancement of the low wavevector fluctuations with no change to the local structure [40]. Experiments were carried out with high angular resolution (approximately 600 data points between $10^{-4} \leqslant q$ (Å^{-1}) $\leqslant 10^{-1}$), and for clarity only alternate data points are reported in this paper. Extensive details of the side-bounce USAXS instrumentation are reported elsewhere [41].

Determination of the colloidal structure factor $S(q)$ requires the accurate measurement of the scattered intensity $I(q)$ from both the suspension of interest and dilute suspensions in the absence of polymer ($\phi_c \sim 0.02 \pm 0.005$) where the measured intensity, $P(q)$, arises from single-particle scattering. Accurate model fits to the $P(q)$ form factor data are imperative in the region of the initial decay of the scattered intensity (0.002 Å$^{-1} < q < 0.01$ Å^{-1}) and the first Bessel function minimum. The largest uncertainty in $P(q)$ determination appears to be in absolute knowledge of q. At q values where $\mathrm{d}P/\mathrm{d}q$ is large, uncertainties of $\pm 20\%$ are anticipated. These uncertainties can give rise to anomalous values of $S(q)$ near the minima of $P(q)$. For this reason the $S(q)$ data are often truncated near $qD = 8$–10 (close to the first minimum in $P(q)$). The large differences between the scattering cross section of the colloid and polymer ensured the scattering yields information about the colloid structure with an immeasurable contribution from the polymer [42].

Least squares fits to the single-particle form factor using equation (1) (normalized to unity) accounts for particle size polydispersity, geometry, and background scattering [43]:

$$P(q, R) = \frac{1}{2\pi\sigma} \int_0^\infty \exp\left(-\frac{(r-R)^2}{2\sigma^2}\right) P^0(q, R) \left(\frac{r}{R}\right)^6 \mathrm{d}r. \tag{1}$$

The model assumes a Gaussian particle size distribution of variance σ, with a mean particle radius R and a form factor $P^0(q, R)$ appropriate for a homogeneous sphere of radius R [43]. Estimates of the standard deviation ($\sim$6%) were in good agreement with both transmission electron microscopy and dynamic light scattering values. To minimize introducing artefacts into the structure factor the model fit to $P(q, R)$ was used to determine $S(q)$ from $I(q)$ data.

3. Polymer reference interaction site model (PRISM) theory

PRISM theory is a generalization to polymers of the small molecule RISM theory of Chandler and Andersen [44–47] based on an interaction site representation of molecules. The novel formulation of PRISM theory to treat thermodynamics, structure and phase separation of mixtures of hard spheres and flexible polymers has been discussed in great depth in recent publications [26, 48–50]. Hence, we only briefly summarize the key aspects relevant to our present applications.

For the binary polymer–particle mixture (the solvent enters implicitly via an effective polymer–polymer interaction), the intermolecular site–site pair correlation functions, $h_{ij}(r) = g_{ij}(r) - 1$, intermolecular site–site direct correlations, $C_{ij}(r)$, and the single molecule structure factors, $\hat{\omega}_i(q)$, are related via the generalized Ornstein–Zernike matrix integral equations which, in Fourier space, are given by [44–47]

$$\hat{h}_{ij}(q) = \hat{\omega}_i(q) \left[\hat{C}_{ij}(q)\hat{\omega}_j(q) + \sum_l \hat{C}_{il}(q)\rho_l \hat{h}_{lj}(q) \right]. \tag{2}$$

The caret denotes Fourier transformed functions with wavevector q and ρ_i is the site number density of species i. For hard spheres, $\hat{\omega}_c(q) = 1$. We employ a field theoretic type model of a polymer chain as a continuous ideal random walk space curve or thread [26, 46] for which

$$\tilde{\omega}_p(q) = \hat{\omega}_p(q)/N = 1/(1 + q^2 R_g^2/2) \tag{3}$$

where N is the degree of polymerization. The ideal random walk model is strictly applicable only under theta solvent conditions, as appropriate for our decalin experiments [5, 50].

The standard atomic Percus–Yevick closure is employed for particle–particle direct correlations [51]. For polymers, the appropriate closure approximation for $C_{pp}(r)$ depends on solvent quality. For the ideal solvent conditions of present interest, on average there are no

inter-polymer interactions due to cancellation of attractive and repulsive interactions. This is modelled in a standard manner by treating polymers as if they can pass through each other, and hence $C_{pp}(r) = 0$ for all separations [27, 50, 52–55]. The possible limitations of this simple description of theta conditions have been discussed in depth elsewhere, where evidence has been given for the adequacy of such a treatment [5, 50]. Finally, the novel modified Percus–Yevick (mPY) closure is employed for polymer–particle direct correlations. The mPY closure properly accounts for, in a self-consistent manner, the non-local loss of conformational entropy when a polymer is near the surface of a hard sphere [26, 48–50]. PRISM-mPY theory has been shown to correctly describe, with quantitative or semi-quantitative accuracy, the fluid–fluid phase separation boundaries, colloid osmotic compressibility and other thermodynamic properties as functions of R_g/R and volume fraction in both ideal (theta) and athermal (good) solvents [3–5, 26, 48]. All calculations presented in this paper are based on the ideal theta solvent version of PRISM theory [5, 50].

The theory also predicts the collective partial structure factors

$$\hat{S}_{ij}(q) = \rho_i \hat{\omega}_i(q)\delta_{ij} + \rho_i \rho_j \hat{h}_{ij}(q) \tag{4}$$

where δ_{ij} is the Kronecker delta function. Direct theoretical comparisons of the PRISM theory colloidal structure factors to the experimental $S(q)$ data (where $S_{cc}(q) = S(q)$) are made in the next section.

4. Colloidal structure factors

Figure 1 shows the phase diagram as a function of the polymer–particle size asymmetry ratio. As discussed in detail previously [5], for $R_g/R < 0.1$ gelation is observed at polymer concentrations *below* the theoretically calculated spinodal boundaries. As the gel boundary is approached from the homogeneous fluid phase with increasing polymer concentration, suspension viscosities tend to diverge and particles are arrested into amorphous configurations. As the gel boundary is crossed the suspensions turn visibly opaque accompanied by a cessation of flow. These effects are observed independent of volume fraction or R_g/R as the gel boundary is crossed. As discussed elsewhere [5], at high ϕ_c the location of the gel boundary is a non-monotonic function of size asymmetry ratio R_g/R. The highest R_g/R sample where gelation was observed experimentally is shown in figure 1.

For $0.1 < R_g/R < 0.3$, stable fluid–crystal transitions are observed and under some conditions a triple gas–fluid–crystal region has been mapped out [13, 14, 27]. For $R_g/R > 0.3$, fluid–fluid transitions are observed at all ϕ_c. However, the phase behaviour is complex for near theta solvent conditions where at high (low) volume fractions the effect of increasing R_g/R leads to a monotonic destabilization (stabilization) of the fluid–fluid binodals [5, 50].

4.1. Length scale dependent colloidal structure

The focus of this paper is $R_g/R \ll 1$ systems at high volume fraction where a direct fluid–gel transition occurs. In the first set of experiments, $R_g/R = 0.053$ and $\phi_c = 0.40 \pm 0.01$. The reduced polymer concentration (c_p/c_p^*) was systematically increased from zero. Conditions were chosen to provide information about structure well into the gel region (i.e. $1 \leqslant c_p/c_p^{gel} \leqslant 3$), where c_p^{gel} is the polymer concentration at the gel boundary.

The measured scattering intensity (normalized by the incident intensity) for two colloid–polymer suspensions in the homogeneous fluid phase is shown in figure 2(A). A least squares fit to the experimental form factor, which is proportional to $P(q)$ in equation (1), is also given. Subsequent figures only include the model form factor fit which was used in the determination

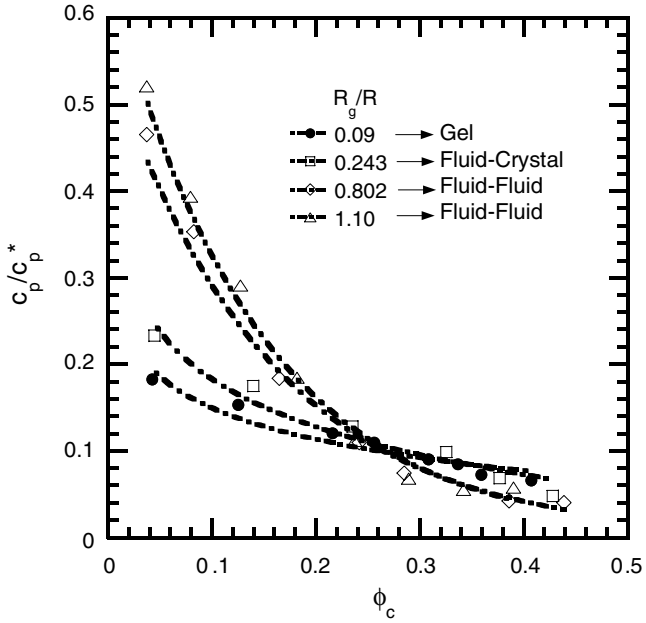

Figure 1. Phase diagram of the silica–polystyrene–decalin mixture at 25 °C for four different size asymmetry ratios (R_g/R) taken from [5]. Symbols represent the experimental phase boundary for $R_g/R = 0.09$ (circles—gel), 0.243 (squares—fluid/crystal), 0.802 (diamonds—fluid/fluid) and 1.10 (triangles—fluid/fluid). Equilibrium phase boundaries are shown as open symbols. The horizontal axis is the colloid volume fraction and the vertical axis is the dimensionless polymer concentration. The curves are drawn to guide the eye.

of the particle structure factor $S(q)$, which in the fluid phase is shown in figure 3(A). The hard sphere data ($c_p/c_p^* = 0$) is also presented for comparison and the excellent fit to the Percus–Yevick theory at such high particle packing fractions is notable. In the homogeneous fluid phase, adding polymer monotonically increases the low angle scattering intensity due to depletion driven clustering of colloids and osmotic compressibility enhancement. The location, q^*, of the first wide angle peak due to local cage order also (weakly) increases with polymer concentration and tends to saturate as the gel boundary is approached. Far from the gel boundary ($c_p/c_p^{gel} < 0.5$) the intensity of the first structure factor peak, $S(q^*)$, initially decreases with polymer concentration. This trend corresponds to the depletion attraction induced 'cage disruption' effect which is central to the physics of the polymer-induced 'colloid glass melting' phenomenon [20–22].

Comparison of the experimental structure factors in the fluid phase with the no adjustable parameter predictions of PRISM-mPY theory is given in figure 3(A). The essentially quantitative agreement extends over a wide q range from length scales that probe the local cage order to large thermodynamic-like scales where the amplitude of the structure factor is controlled by the osmotic compressibility. As documented in our previous studies [4, 5, 28], at elevated polymer concentrations approaching the gelation boundary PRISM theory weakly under-predicts the long wavelength consequences of depletion attractions and colloidal clustering. However, near-quantitative agreement is observed even at $qD \sim 0.5$ (figure 3(A)).

Excellent agreement between theory and experiment holds below the gel boundary corresponding to the $c_p/c_p^* < 0.1$ (figure 3(A)). In the gel (figure 3(B)), the peak intensity is larger than at $c_p/c_p^* = 0.02$ and 0.05. The non-monotonic dependence of the cage order

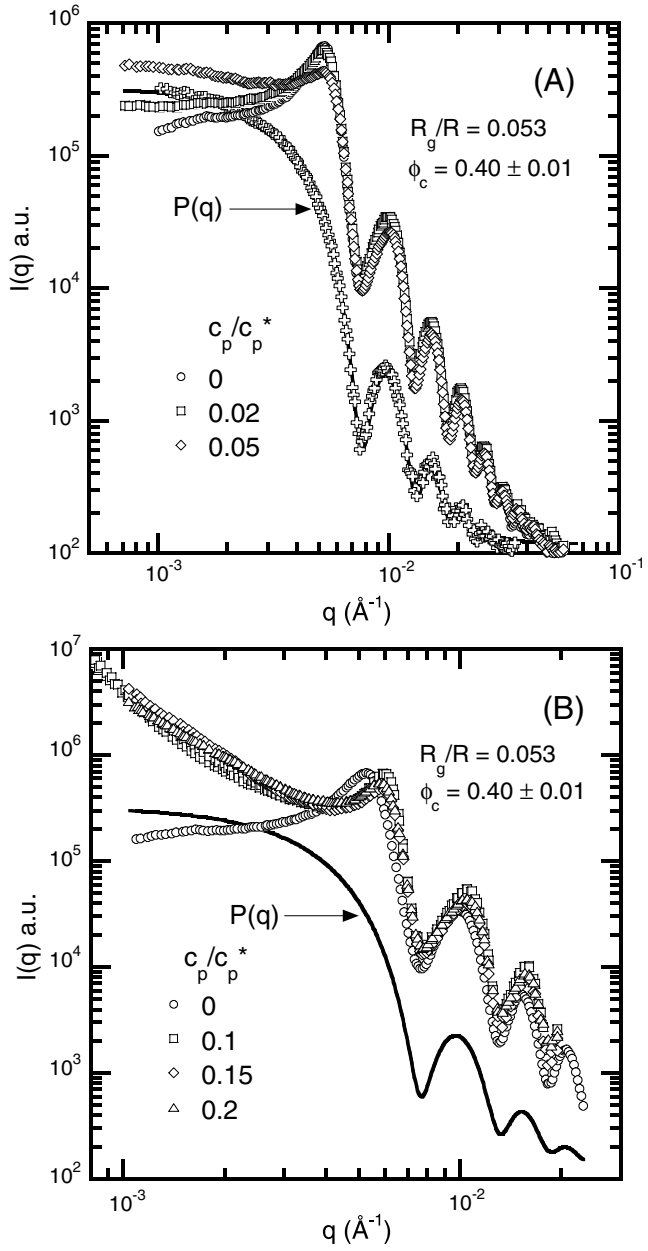

Figure 2. (A) Normalized scattering intensities $I(q)$ as a function of q (Å^{-1}) for liquid samples with varying amounts of polymer quantified by the dimensionless polymer concentration c_p/c_p^*. The colloid volume fraction is fixed at $\phi_c = 0.40 \pm 0.01$ and $R_g/R = 0.053$. Data are shown for $c_p/c_p^* = 0$ (circles), 0.02 (squares) and 0.05 (diamonds). Experimental data (crosses) and a model fit (full curve) for $P(q)$ are shown for comparison. (B) Normalized scattering intensities $I(q)$ as a function of q (Å^{-1}) for gel samples with varying amounts of polymer: $c_p/c_p^* = 0.1$ (squares), 0.15 (diamonds) and 0.2 (triangles) for the same ϕ_c and R_g/R as (A). The pure hard sphere result (circles) is also shown.

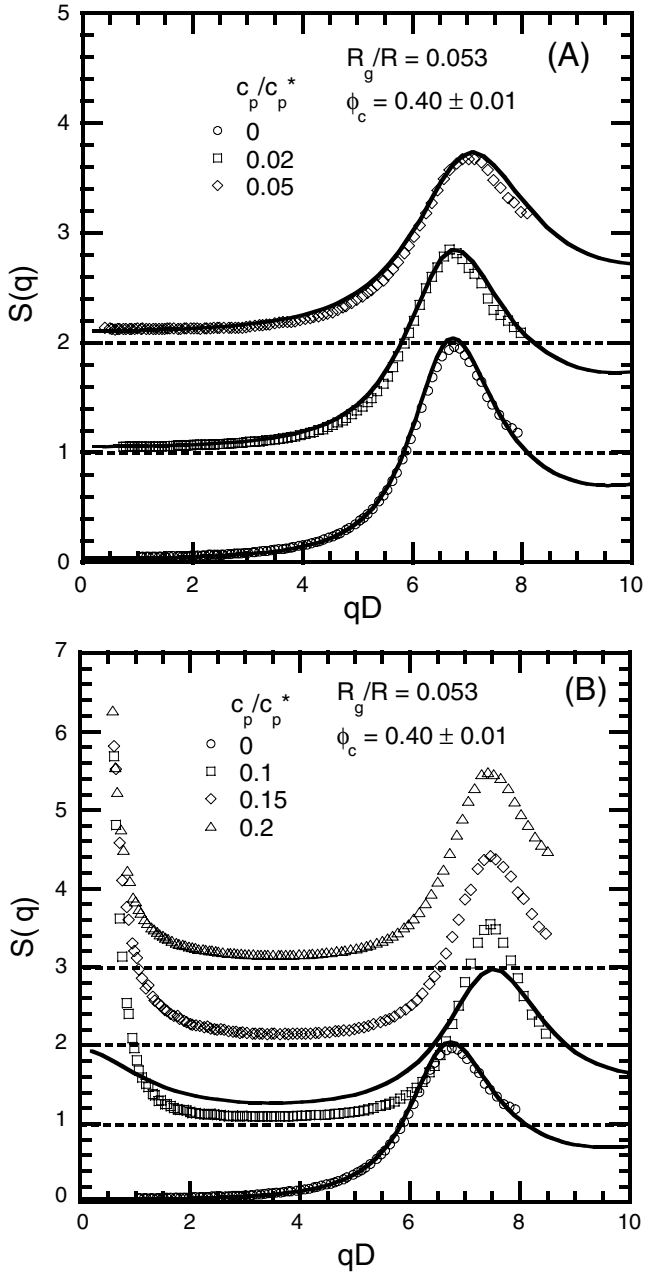

Figure 3. Structure factor $S(q)$ as a function of the dimensionless wavevector qD for samples with varying amounts of polymer quantified by the dimensionless polymer concentration, c_p/c_p^*. The colloid volume fraction is fixed at $\phi_c = 0.40 \pm 0.01$ and $R_g/R = 0.053$. (A) Liquid samples: $c_p/c_p^* = 0$ (circles), 0.02 (squares) and 0.05 (diamonds). (B) Gel samples: $c_p/c_p^* = 0.1$ (squares), 0.15 (diamonds) and 0.20 (triangles), and as a reference $c_p/c_p^* = 0$ (circles). Each subsequent data set is offset by 1 for clarity. Dotted lines show relevant baselines signifying $S(q) = 0$ for each data set. Full curves are the zero-adjustable parameter PRISM-mPY theory predictions.

parameter, $S(q^*)$, on polymer concentration in the fluid phase has been previously reported and analysed in depth both theoretically [26] and experimentally for polymer–colloid suspensions with $R_g/R = 0.06$ in good and theta solvents [28]. In the latter study, and for the data of figure 3, the magnitude of the first peak at the gelation transition is, perhaps coincidentally, close to (or slightly greater than) the polymer-free hard sphere fluid value.

Figure 3(B) also shows that the cage peak intensity and location are nearly independent of polymer concentration in the gel phase. This apparent 'freezing' of the local structure has been previously reported from neutron scattering studies on polymer-free thermoreversible gels of adhesive colloids which interact via short-range attractions [40]. In contrast to the cage scale behaviour, on intermediate length scales, $1.5 < qD < 5$, the experimental $S(q)$ in the gel is significantly smaller than predicted by the equilibrium theory. This suggests on the ∼2–4 particle diameter length scale the nonequilibrium gel structure is less compressible, and locally denser, than it would be if the system was in thermodynamic equilibrium. Large amplitude, long wavelength fluctuations also emerge in the gel, presumably indicative of some type of quenched disorder or heterogeneity. The smallest q values reported are within the angular resolution limit of the instrument.

Over all the wavevectors probed, which extend out to real space length scales of about 30 colloid diameters, the structure factors in the gel are nearly independent of polymer concentration. The gradient of the low angle upturn of $S(q)$ is quite similar for $1 \leqslant c_p/c_p^{gel} < 3$, implying that the origin of the sharp increase in the low angle scattering is insensitive to the strength of attraction. These features emphasize the nonequilibrium nature of the structural reorganization in the gel and the irrelevance (to a first approximation) of any buried fluid–fluid spinodal or other metastable equilibrium phase boundaries. This situation appears to be in contrast with prior studies of polymer–colloid gels, which were created by quenching lower volume fraction suspensions (often deeply) into a metastable two-phase region [2, 56–59]. For such systems, gelation is more complex due to its coupling with a spinodal decomposition and/or nucleation and growth phase separation process.

The large increases in $S(q)$ at low q have also been shown to coincide with abrupt changes in the dynamic structure factor (loss of ergodicity) [39]. Experiments with thermoreversible gels of adhesive spheres find the low angle static structure factor to continuously increase for $\varepsilon_T = (T - T_{gel})/T_{gel} > 1$ where T_{gel} is the temperature at which the suspensions gel. The relative distance from the gel boundary in [39] was controlled by small changes in the temperature ($\varepsilon_T \pm 1 \times 10^{-4}$) allowing for a gradual entry into the gel state. In the present study, comparable tiny changes in polymer concentration $\varepsilon_c = (c_p - c_p^{gel})/c_p^{gel}$ were not attempted.

4.2. Effect of size asymmetry

The structural consequences of increasing R_g/R from 0.053 to 0.078 were explored at the same fixed colloid volume fraction of $\phi_c = 0.40 \pm 0.01$ for liquid (figures 4(A) and 5(A)) and gel samples (figures 4(B) and 5(B)). Quantitative differences are evident. However, the effect of polymer additives on colloidal structure is qualitatively identical to the behaviour of the $R_g/R = 0.053$ mixture. Hence, the pattern of behaviour described in section 4.1 appears to be generic for high volume fraction polymer–colloid mixtures where the effective range of the depletion potential is small. In particular, the cage coherence parameter, $S(q^*)$, is again a non-monotonic function of c_p/c_p^*, first decreasing and then increasing as $c_p/c_p^{gel} > 0.7$.

For the equilibrium fluid samples, excellent quantitative agreement of experiment with PRISM theory is again found. The predicted spinodal boundary occurs at a moderately higher reduced polymer concentration ($c_p^{spin}/c_p^* \sim 0.13$) for the $R_g/R = 0.078$ mixture compared to the $R_g/R = 0.053$ system ($c_p^{spin}/c_p^* \sim 0.11$).

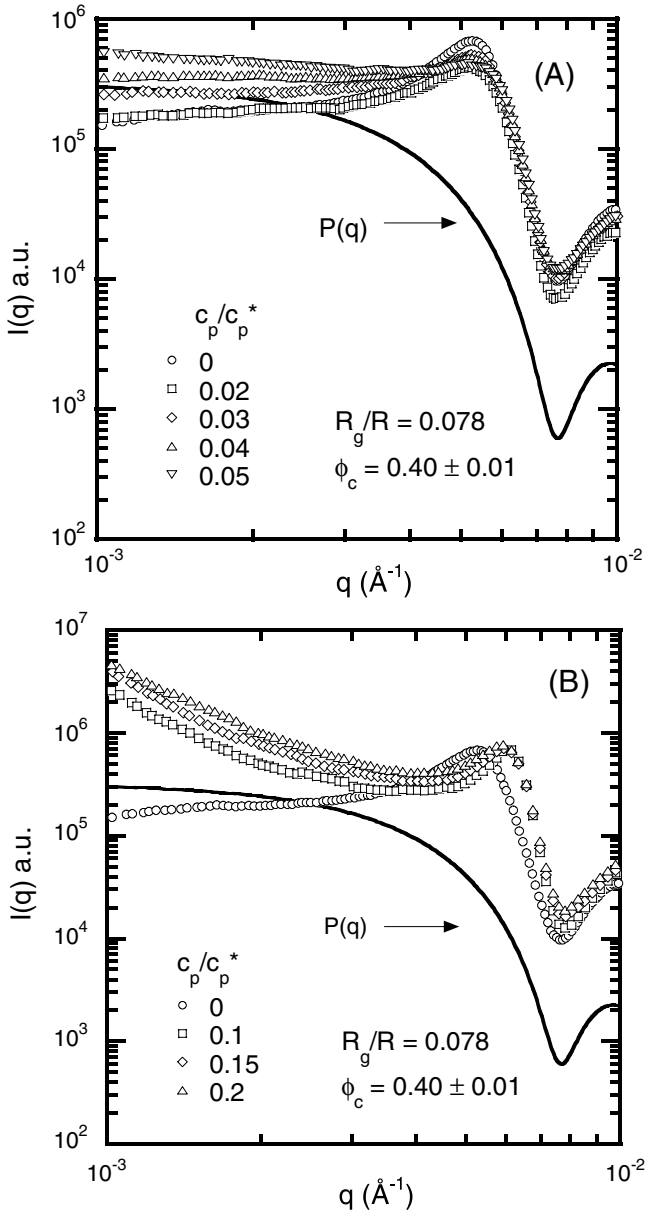

Figure 4. (A) Normalized scattering intensities $I(q)$ as a function of q (Å^{-1}) for liquid samples with varying amounts of polymer quantified by the dimensionless polymer concentration c_p/c_p^*. The q range shown is limited to $1 \times 10^{-3} \leqslant q \leqslant 1 \times 10^{-2}$ (Å^{-1}) for clarity. The colloid volume fraction is fixed at $\phi_c = 0.40 \pm 0.01$ and $R_g/R = 0.078$. Data are shown for $c_p/c_p^* = 0$ (circles), 0.02 (squares), 0.03 (diamonds), 0.04 (triangles) and 0.05 (inverted triangles). (B) Normalized scattering intensities $I(q)$ as a function of q (Å^{-1}) for gel samples with varying amounts of polymer: $c_p/c_p^* = 0.1$ (squares), 0.15 (diamonds) and 0.2 (triangles) for the same ϕ_c and R_g/R as (A). The pure hard sphere result (circles) is also shown. Model fit for $P(q)$ (full curve) is shown for comparison.

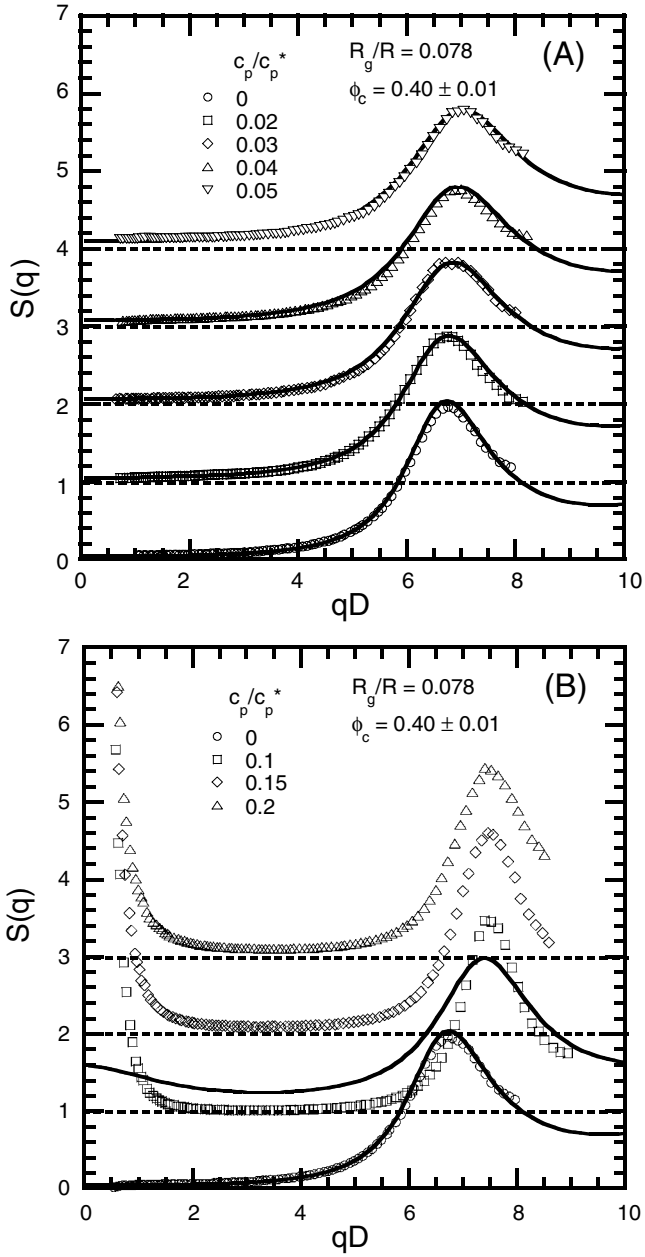

Figure 5. Structure factor $S(q)$ as a function of the dimensionless wavevector qD for samples with varying amounts of polymer quantified by the dimensionless polymer concentration, c_p/c_p^*. The colloid volume fraction is fixed at $\phi_c = 0.40 \pm 0.01$ and $R_g/R = 0.078$. (A) Liquid samples: $c_p/c_p^* = 0$ (circles), 0.02 (squares), 0.03 (diamonds), 0.04 (triangles) and 0.05 (inverted triangles). (B) Gel samples: $c_p/c_p^* = 0.1$ (squares), 0.15 (diamonds) and 0.20 (triangles), and as a reference $c_p/c_p^* = 0$ (circles). Each subsequent data set is offset by 1 for clarity. Dotted lines show relevant baselines signifying $S(q) = 0$ for each data set. Full curves are the zero-adjustable parameter PRISM-mPY theory predictions.

Theory and experiment increasingly disagree as the gel state is entered ($c_p^{gel}/c_p^* \sim 0.09 \pm 0.01$). Suppressed concentration fluctuations on intermediate $1.5 < qD < 5$ scales, and a strong enhancement for $qD \leqslant 1.5$, is again observed. Within experimental uncertainties, both the local and intermediate length scale structures appear essentially frozen in the gel phase. In contrast to samples in equilibrium, structure appears to be insensitive to changes in R_g/R.

4.3. Effect of volume fraction

One additional set of experiments probed the effects of modestly changing particle volume fraction for the $R_g/R = 0.053$ system by employing a larger $\phi_c = 0.45 \pm 0.01$. Results in the fluid and gel states are given in figures 6 and 7. The reduced polymer concentrations are very similar to those utilized for the analogous $\phi_c = 0.40$ system (see table 1). The PRISM theory spinodal boundary at $\phi_c = 0.45$ is $c_p^{spin}/c_p^* \sim 0.11$, and experimentally gelation occurs at $c_p^{gel}/c_p^* \sim 0.09 \pm 0.01$.

In the absence of polymer, a higher particle volume fraction results in an increase of the local cage order parameter, $S(q^*)$, and reduction of the low angle intensity. The influence of polymer additives is quantitatively amplified at the higher volume fraction. This is clear from figure 7(A) where there is a distinct departure between the measured and predicted $S(q)$ at small wavevectors for $c_p/c_p^* = 0.05$. In contrast, at the same polymer concentration at $\phi_c = 0.40$ (see figure 3(A)) the agreement between experiment and theory remains excellent due to the smaller depletion-driven compressibility enhancement at the lower volume fraction. As ϕ_c increases, the addition of polymer initially suppresses $S(q^*)$ more strongly, indicating quantitatively larger alterations of the cage structure by depletion attractions (figure 7(A)). When the gel boundary is crossed the changes in the scattering patterns are qualitatively the same as found for the lower volume fraction.

5. Structural reorganization on the cage scale

Figures 8 and 9 summarize the changes to the cage order parameter $S(k^*)$ and dimensionless peak position $k^* = q^*D$ for all three systems. For purposes of comparison we also include our recently reported results for the analogous $R_g/R = 0.06$ suspensions in decalin for which $c_p^{gel}/c_p^* \sim 0.095$ [28]. At the high ϕ_c of present interest, the gel boundaries are relatively insensitive to both volume fraction and spatial range of the depletion attraction.

All samples initially show a decrease in $S(k^*)$ with increasing c_p/c_p^*, followed by an upturn before an abrupt freezing of the local structure associated with gel formation. The characteristic cage wavevector (k^*) increases monotonically with polymer concentration by $\sim$15% in the fluid phase, and then appears to arrest in the gel. PRISM theory predictions of $S(k^*)$ and k^* are in very good agreement with experiment for all fluid samples. The abrupt departure from theory at the gel transition provides strong evidence for the samples 'falling out' of equilibrium. Not surprisingly, the structural arrest coincides with a plateau in the value of k^* where the average spacing between particles becomes a weak function of the strength of attractions. Since the experimental values of k^* for liquid samples agree quantitatively with PRISM predictions, the origin for the saturation is likely due to the localization of particles in contact in the gel.

Interestingly, the insensitivity to polymer concentration of gel structure on the observable length scales does not correlate with viscoelastic properties of depletion flocculated gels. For example, the gel elastic shear modulus does increase with the depletant concentration [8, 60, 61]. This suggests that density–density correlations on the particle (and

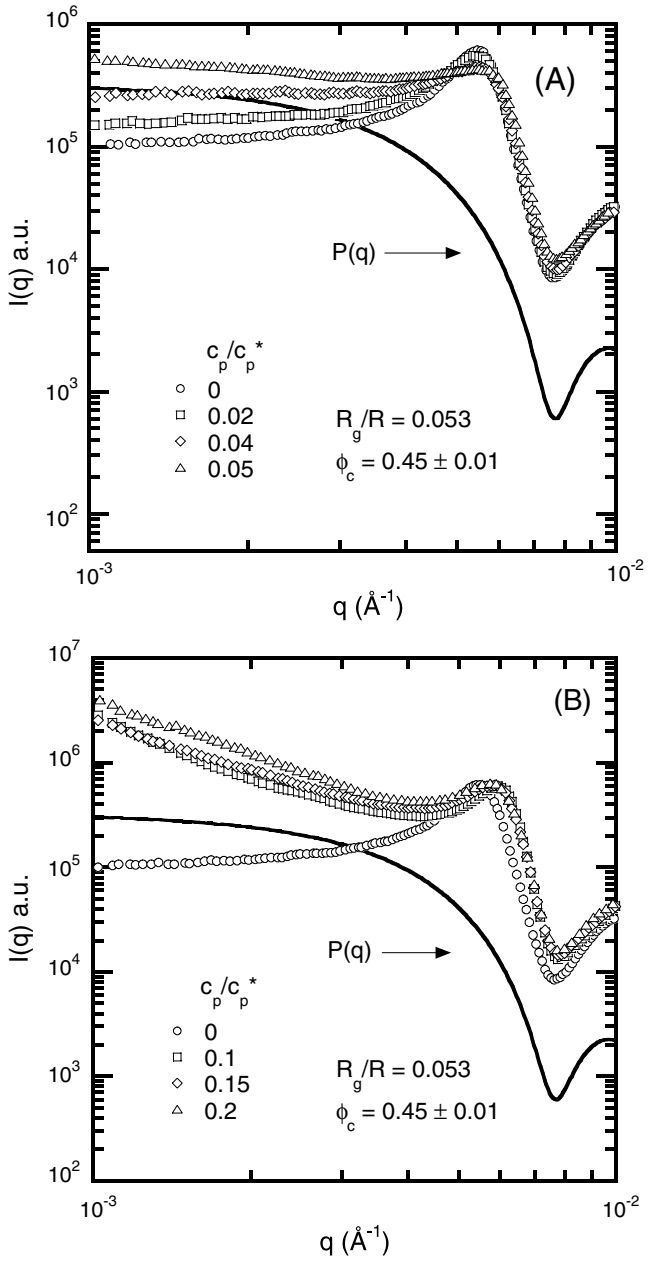

Figure 6. (A) Normalized scattering intensities $I(q)$ as a function of q (Å^{-1}) for liquid samples with varying amounts of polymer quantified by the dimensionless polymer concentration c_p/c_p^*. The q range shown is limited to between $1 \times 10^{-3} \leqslant q \leqslant 1 \times 10^{-2}$ (Å^{-1}) for clarity. The colloid volume fraction is fixed at $\phi_c = 0.45 \pm 0.01$ and $R_g/R = 0.053$. Data are shown for $c_p/c_p^* = 0$ (circles), 0.02 (squares), 0.04 (diamonds) and 0.05 (triangles). (B) Normalized scattering intensities $I(q)$ as a function of q (Å^{-1}) for gel samples with varying amounts of polymer: $c_p/c_p^* = 0.1$ (squares), 0.15 (diamonds) and 0.2 (triangles) for the same ϕ_c and R_g/R as (A). The pure hard sphere result (circles) is also shown. Model fit for $P(q)$ (full curve) is shown for comparison.

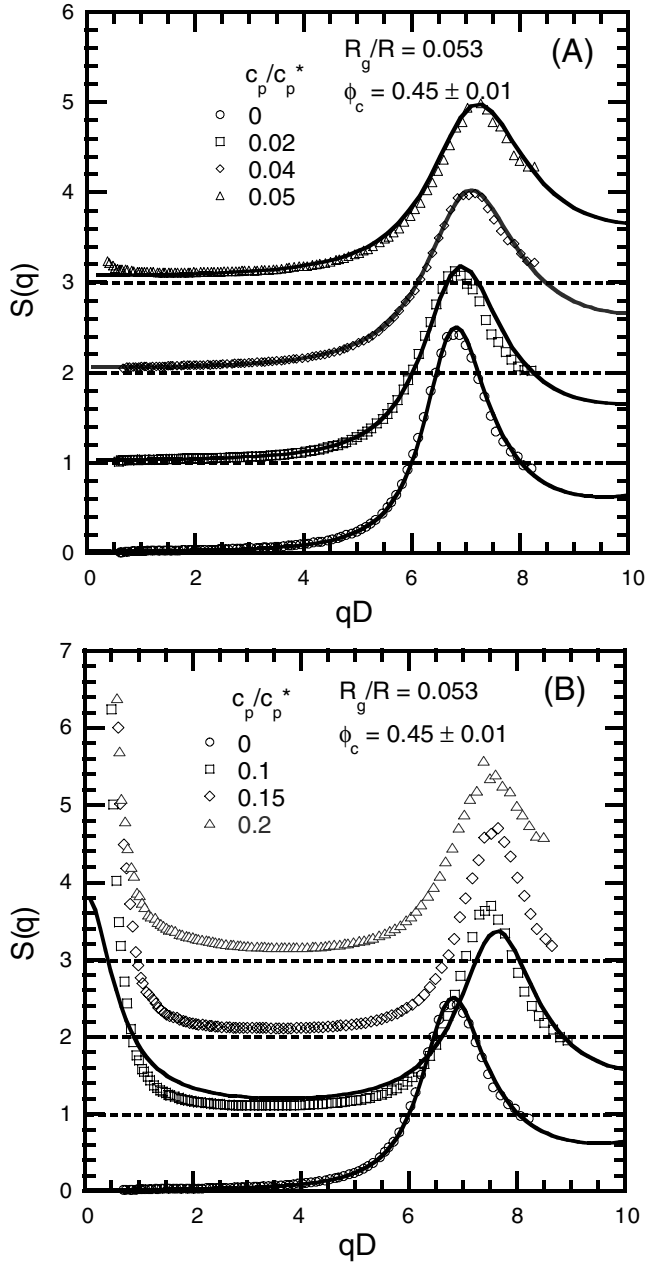

Figure 7. Structure factor $S(q)$ as a function of the dimensionless wavevector qD for samples with varying amounts of polymer quantified by the dimensionless polymer concentration, c_p/c_p^*. The colloid volume fraction is fixed at $\phi_c = 0.45 \pm 0.01$ and $R_g/R = 0.053$. (A) Liquid samples: $c_p/c_p^* = 0$ (circles), 0.02 (squares), 0.04 (diamonds) and 0.05 (triangles). (B) Gel samples: $c_p/c_p^* = 0.1$ (squares), 0.15 (diamonds) and 0.20 (triangles), and as a reference $c_p/c_p^* = 0$ (circles). Each subsequent data set is offset by 1 for clarity. Dotted lines show relevant baselines signifying $S(q) = 0$ for each data set. Full curves are the zero-adjustable parameter PRISM-mPY theory predictions.

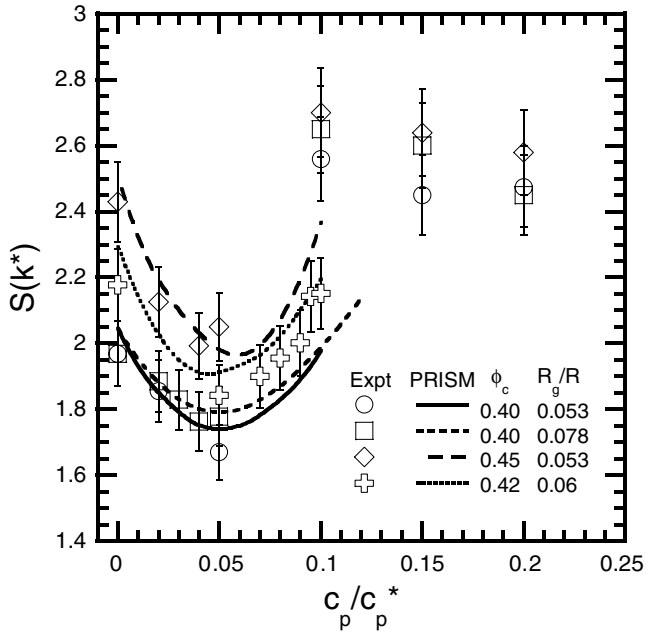

Figure 8. Magnitude of the structure factor at the position of the first peak, $S(k^*)$, as a function of the dimensionless polymer concentration c_p/c_p^* for $R_g/R \sim 0.053$ and $\phi_c = 0.40$ (circles), $R_g/R = 0.078$ and $\phi_c = 0.40$ (squares), and for $R_g/R \sim 0.053$ and $\phi_c = 0.45$ (diamonds) for both the liquid and gel states. For comparison, data from [28] for $S(k^*)$ in decalin (crosses) at $R_g/R \sim 0.06$ are also shown. The corresponding PRISM-mPY theory predictions are shown as curves.

larger) length scale may not strongly affect the gel rheological response, in agreement with the combined SANS and rheological study of Rueb *et al* [40]. A caveat to these deductions is the accuracy to which one can experimentally measure small changes in structure in the gel, and how large a structural change will impact the mechanical properties. At a fixed particle volume fraction, the present data do suggest there is a weak effect of changing the range of interparticle attractions in both the fluid and gel phase. Based on the idealized mode-coupling theory (MCT), the important length scale is proportional to the range of the depletion attraction [19, 20, 62]. This corresponds to $qD \gg 10$ which is beyond what can be probed in the present systems by x-ray scattering.

6. Intermediate scale fluctuations, low angle upturn and heterogeneities in gels

6.1. Intermediate length scales

We define 'intermediate' wavevectors as $1.5 < qD < 4$, corresponding to collective structure on the ∼2–4 particle diameter length scale. As seen from figures 3(B), 5(B) and 7(B), the shape of $S(q)$ on these scales retain their liquid-like character, even for $c_p > c_p^{gel}$. This suggests that the large scale heterogeneities that are presumably the origin of the small angle upturns in scattering play a minor role on these intermediate scales.

A summary of the behaviour of all three systems at a reduced intermediate wavevector of $qD = 2$ is shown in figure 10. In the fluid phase, the amplitude of fluctuations monotonically increase with polymer concentration. This reflects finite length scale consequences of depletion

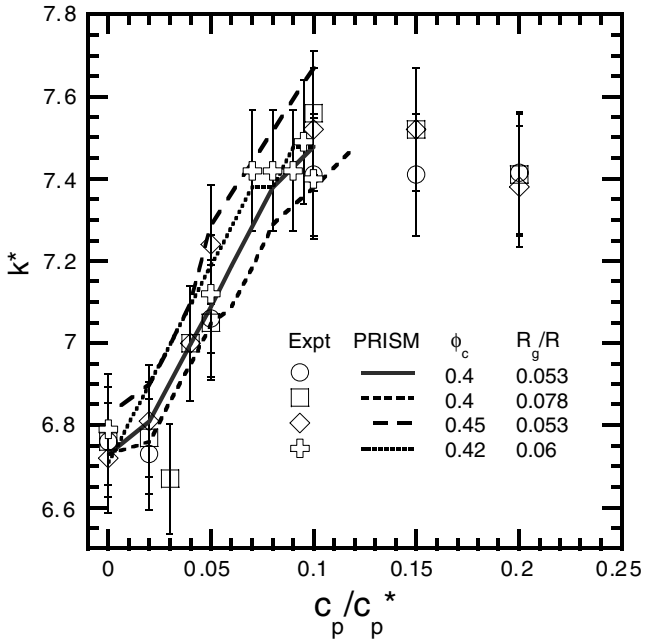

Figure 9. Position of the first peak k^* as a function of reduced polymer concentration c_p/c_p^* for $R_g/R \sim 0.053$ and $\phi_c = 0.40$ (circles), $R_g/R = 0.078$ and $\phi_c = 0.40$ (squares), and $R_g/R \sim 0.053$ and $\phi_c = 0.45$ (diamonds) corresponding to the data in figure 8. For comparison, data from [28] for k^* in decalin (crosses) at $R_g/R \sim 0.06$ are also shown. The corresponding PRISM-mPY theory predictions are shown as curves.

driven colloidal clustering, which is well accounted for by PRISM theory. However, as the gel boundary is traversed, there are abrupt wavevector dependent departures from the equilibrium theory.

On the ∼3 particle length scale ($qD = 2$), a large suppression of fluctuations is evident from figure 10. The amplitude of fluctuations is a factor of about 2–4 times smaller than expected for the equilibrium fluid. Moreover, the relative ordering of $S(q)$ does not follow its fluid phase, or equilibrium theory, trend. As the gel state is entered more deeply, fluctuations appear to weakly increase. This could be due to nonequilibrium, local compaction processes and/or a small influence of the metastable phase separation boundaries. Inspection of figures 3(B), 5(B) and 7(B) show the above trends also hold for $qD \sim 3$ corresponding to fluctuations on a ∼2 particle length scale.

6.2. Low angle scattering and possible morphological models

The most pronounced feature of the gel state observed from USAXS is the sharp upturn of the low wavevector intensity. For a fixed particle size, within our limited ability to make measurements at the lowest q, the gel data are reliable down to $qD \sim 0.25$. The dramatic enhancement of long wavelength fluctuations on the ∼6–30 particle diameter length scales suggests the existence of heterogeneities or 'voids', as recently observed using confocal microscopy in dense suspensions of attractive adhesive particles [30]. Characterization and understanding of the physical nature of the entities which produce such scattering is difficult, especially at high volume fractions. In this section we consider various possible interpretations.

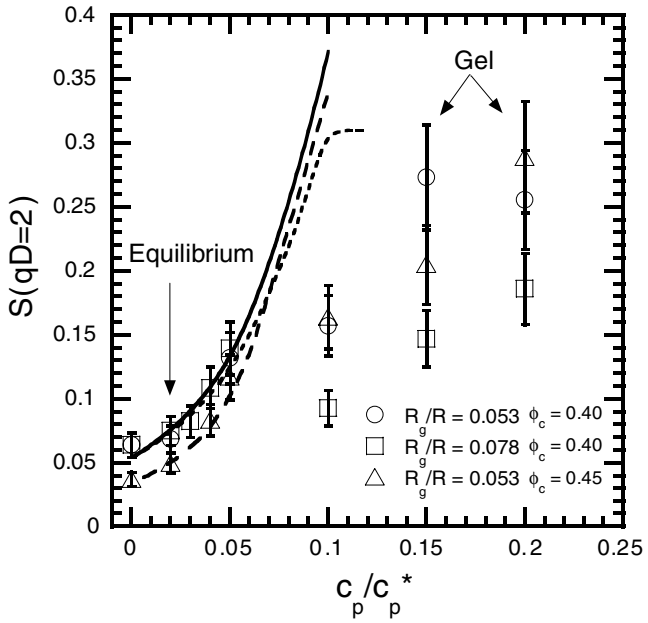

Figure 10. Structure factor at a fixed value of the dimensionless wavevector $qD = 2$ as a function of c_p/c_p^* for $R_g/R \sim 0.053$ and $\phi_c = 0.40$ (circles), $R_g/R = 0.078$ and $\phi_c = 0.40$ (squares) and $R_g/R \sim 0.053$ and $\phi_c = 0.45$ (triangles). The corresponding PRISM-mPY theory predictions are shown as full, dotted and broken curves, respectively.

The upturn of $S(q)$ at low q in the gel could possibly arise from equilibrium concentration fluctuations as the fluid–fluid spinodal boundary is approached. This explanation appears unlikely for at least three reasons.

(1) The apparent freezing of the equilibrium structural correlations at $c_p > c_p^{gel}$.
(2) The abruptness and magnitude of the upturn seen experimentally are not consistent with theoretical expectations for fluid–fluid phase separation.
(3) For the small values of R_g/R studied, the strong upturn feature emerges at polymer concentrations well below the calculated spinodal boundaries, as discussed in sections 4.2 and 4.3, and elsewhere [3, 5].

Gelation of low particle volume fraction suspensions (typically $<10\%$) is often interpreted as a kinetic process due to the aggregation and close packing of fractal clusters [2, 58, 63]. The latter are identified experimentally from a power law increase in scattering intensity at low q [64]. At very low wavevectors, a peak in $S(q)$ is sometimes observed [2, 57, 58, 65], but alternatively a high plateau is also often observed [39, 66]. Based on the former behaviour, gelation is argued to occur when the fractal clusters formed by a diffusion-limited cluster–cluster aggregation (DLCA) process begin to jam and/or stick to form a space-spanning network [2, 57, 65]. Alternatively, for thermoreversible gels at low ϕ_c, a number of studies have found that the low angle scattering can be fitted as $S(q) \sim (q^2 + \xi^2)^{-d_f/2}$, where fractal dimensions of $d_f \sim 2.2 \pm 0.2$ are commonly extracted [39, 66, 67].

At the high volume fractions of present interest, a fractal cluster model in the classic sense is not very plausible. Moreover, we do not observe either a low angle peak, nor a low angle plateau in $S(q)$. What seems more likely is the emergence of dense, small 'clusters' or aggregates formed via effectively irreversible sticky collisions. Such entities may be more compact than

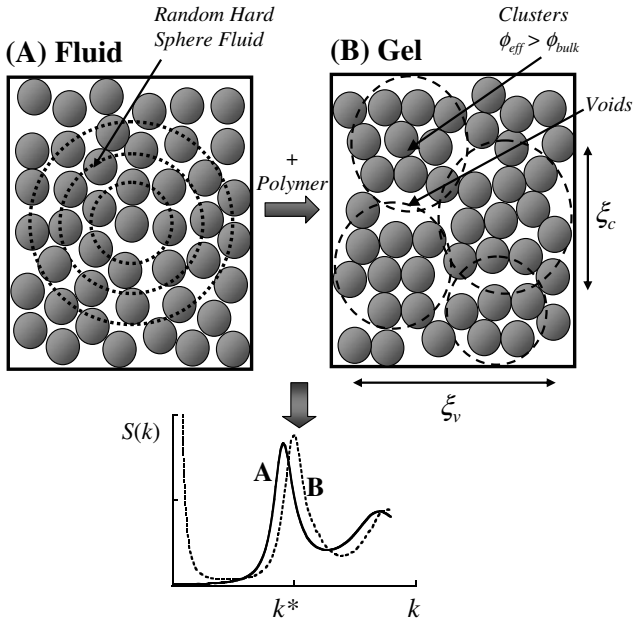

Figure 11. An illustration of (A) a hard-sphere fluid and (B) interpenetrating, polydisperse, dense percolated clusters of an average size ξ_c. The surrounding voids or heterogeneities have a characteristic length of $\xi_v \sim 5$–$8D$ where D is the colloid diameter. Also shown is a schematic illustrating changes in the structural correlations as equilibrium fluids transform to dense gels.

those based on global equilibrium considerations due to locally reversible rearrangements. The suppressed fluctuations we observe (figures 3(B), 5(B), 7(B) and 10) in the gel state on a 'cluster' size scale of $\xi_c \sim 3$–$4D$ is consistent with this idea. Local densification is also supported by our observation in the gel of an increased cage order parameter, $S(k^*)$, which exceeds the hard-sphere suspension value. Such small 'clusters' may have fractally rough surfaces, and are likely to be polydisperse and interpenetrating to some degree in order to maintain the mechanical integrity of the material. If local compaction occurs in the gel, mass conservation would require the creation of some 'free volume', 'voids' or heterogeneities, likely percolated, which could be the origin of the low angle upturn. The overall gel would thus be envisioned as a random 'two-phase' composite, with a proliferation of internal 'interfaces'. However, the elementary length of such 'free volume' would be very small, being controlled by the range of the depletion attraction which is of the order of $R_g \ll R$. An illustration of a possible microstructural model is given in figure 11.

To investigate the possible relevance of the above qualitative idea for the gel microstructure, our low angle scattering data is plotted in a log–log format in figure 12. Clearly the upturn does not imply fractal clusters, since the extracted exponents all exceed the dimension of space. Rather, we find a $\sim q^{-3.5\pm0.3}$ power law, more characteristic of a Porod-like decay ($\sim q^{-4}$) appropriate for objects with sharp interfaces. In three dimensions, scattering from compact objects with fractally rough surfaces also follow a power law with an exponent greater than 3 and less than 4 [68]. There appears to be no systematic differences in the slopes for the various gel samples as a function of either R_g/R or ϕ_c. The Porod-like behaviour breaks down at higher wavevectors, roughly beyond $qD \sim 1.5$–2. There is a crossover to a more flat, liquid-like response on the $\xi_c \sim 3$–4 particle diameter length scale, with an amplitude suppressed relative to equilibrium considerations.

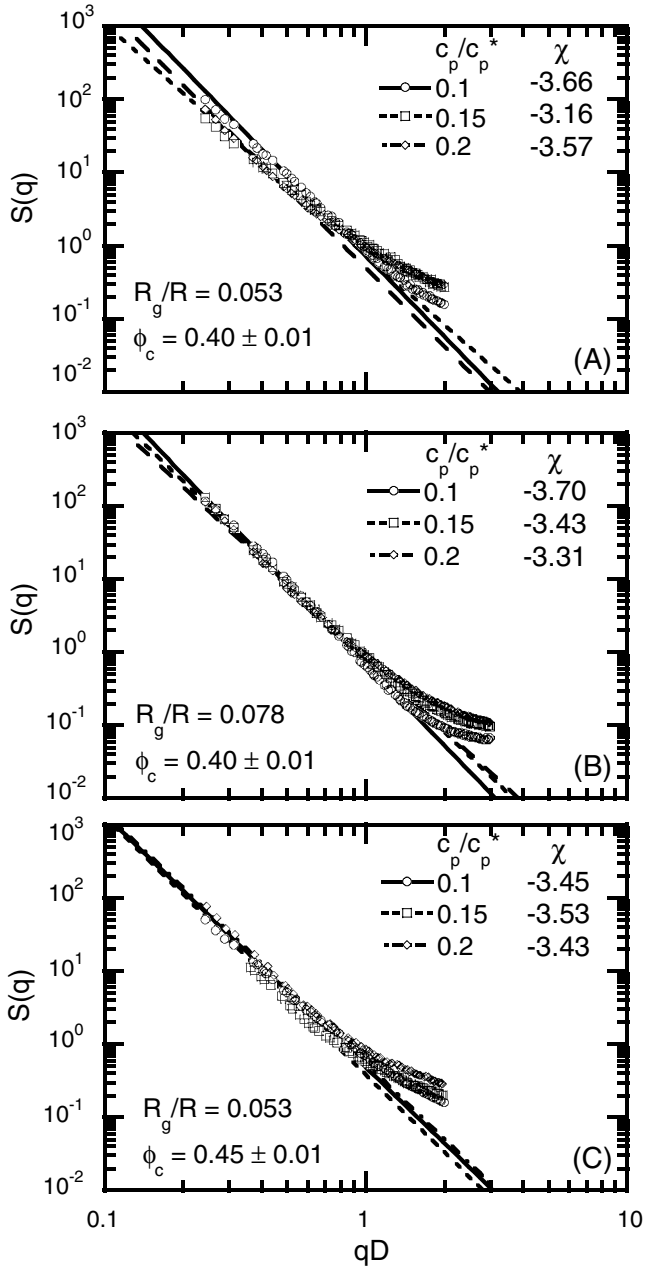

Figure 12. Log–log plot of the low angle structure factor of the gel samples at $c_p/c_p^* = 0.1$ (circles), 0.15 (squares) and 0.2 (diamonds) for the following conditions: (A) $R_g/R = 0.053$, $\phi_c = 0.40$; (B) $R_g/R = 0.078$, $\phi_c = 0.40$ and (C) $R_g/R = 0.053$, $\phi_c = 0.45$. Lines are power law fits to the data with the best fit slopes indicated as χ.

6.3. Debye–Bueche analysis

Porod-like small-angle scattering has been observed in a variety of different polymeric materials, including crosslinked gels, polyelectrolyte solutions, ionomer melts and

semicrystalline polymers [69–73]. A common interpretation is that there is some kind of random nonequilibrium disorder or heterogeneities that are frozen in the material. These provide strong low angle scattering intensity, which is superimposed on a 'regular' part of the scattering which arises from smaller length scale fluctuations of either equilibrium, or near-equilibrium, origin. This physical picture seems plausible for our colloidal gel system and consistent with the illustration in figure 11.

A generic 'random two-phase' model often employed to describe scattering from quenched structural heterogeneities is due to Debye and Bueche [74]. A random distribution of heterogeneities is modelled via a characteristic size (or separation) ξ_v, and a corresponding amplitude quantified via a dimensionless fluctuation parameter $\langle\eta^2\rangle$. In real space, the heterogeneity distribution function, or density–density correlation function, is given by

$$\rho\gamma(r) = \langle\eta^2\rangle \exp\left(\frac{-r}{\xi_v}\right). \tag{5}$$

For our system, $\langle\eta^2\rangle = \langle(\delta\rho)^2\rangle/\rho^2$ represents the dimensionless mean square number density difference between the 'dense clusters' and the 'voids', and the mean colloidal number density is ρ. The corresponding dimensionless Debye–Bueche scattering function is

$$S_{D-B}(q) = \frac{S_{D-B}(0)}{(1+q^2\xi_v^2)^2} \tag{6a}$$

$$S_{D-B}(0) = 48\phi_c\left(\frac{\xi_v}{D}\right)^3\langle\eta^2\rangle. \tag{6b}$$

The total structure factor is given by $S(q) = S_{D-B}(q) + S_c(q)$.

The appropriateness of this model for describing the low angle upturn region of the gel structure factor can be tested by plotting $S(qD)^{-1/2}$ versus $(qD)^2$. If a straight line is found (over a limited q range), the parameters $S_{D-B}(0)$ and ξ_v can be extracted. Figures 13(A)–(C) show that reasonable fits can be obtained, with correlation lengths of $\xi_v \sim 5$–8 particle diameters and $S_{D-B}(0) \sim 300$–800. As indicated in figure 13, the experimental uncertainties in ξ_v are significant. We find no systematic variations in ξ_v as a function of R_g/R, c_p/c_p^* and/or ϕ_c. The value of $S_{D-B}(0)$ due to the heterogeneities is roughly two orders of magnitude larger than its 'intra-cluster' analogue, estimated as $S_c(0) \approx S(qD \sim 2) \sim 0.2$ (see figure 10).

Are the Debye–Bueche fit parameters physically reasonable and consistent with the qualitative microstructure model of figure 11? A length scale of ∼5–8 particle diameters seems plausible as a characteristic distance between small void spaces surrounding the denser regions ('clusters') of size $\xi_c \sim 3$–$4D$. From $S_{D-B}(0) \sim 300$–800, $\xi_v \sim 5$–$8D$, and equation (6*b*), an estimate of the dimensionless ratio of the quenched density fluctuation amplitude is obtained as $\langle\eta^2\rangle \sim 0.05$–$0.2$. This is a physically realizable value and is small, consistent with expectations for a high suspension volume fraction and a short range depletion attraction. For comparison, $\langle\eta^2\rangle \sim 0.04$ at $\phi_c = 0.40$ for a hard-sphere fluid. Hence, this analysis is suggestive that the high intensity small-angle scattering is the result of a large correlation length of the (perhaps percolating) void space which constitutes the heterogeneity.

6.4. Fractal cluster model

To explore alternative interpretations, we use standard fractal arguments to estimate a 'cluster' length scale. Given the relatively weak and isotropic nature of depletion attractions between hard-sphere colloids, significant 'bond bending' between particles seems likely in the gel state.

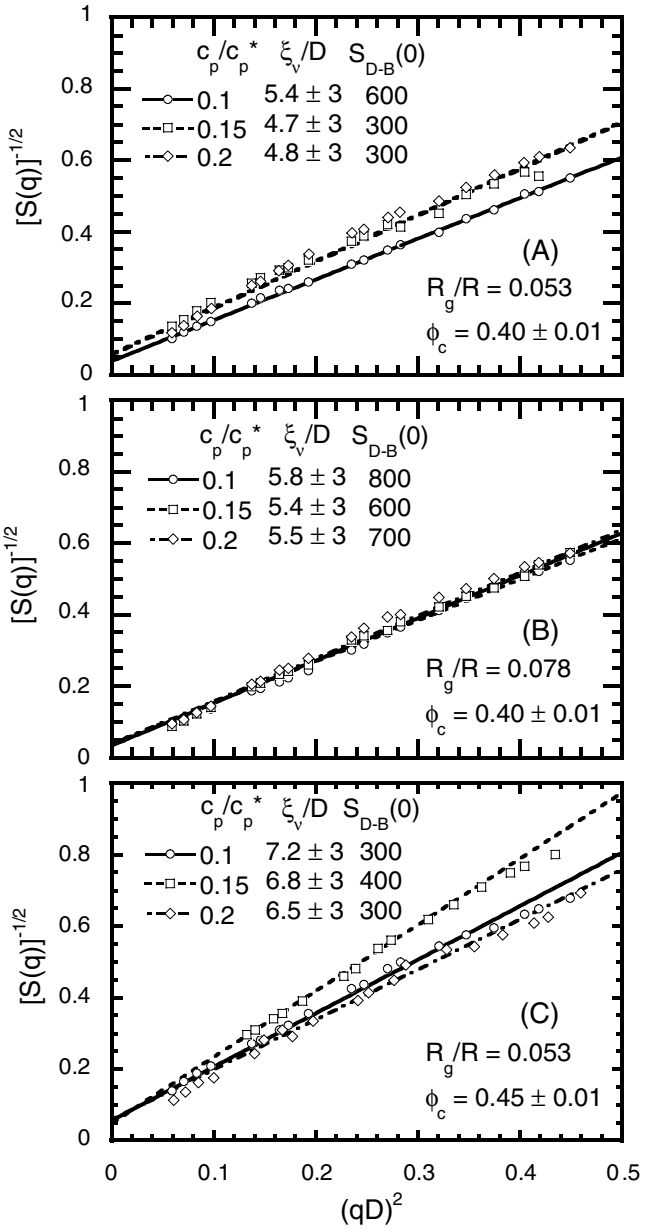

Figure 13. Debye–Bueche plots for gel samples at $c_p/c_p^* = 0.1$ (circles), 0.15 (squares) and 0.2 (diamonds) for the following conditions: (A) $R_g/R = 0.053$, $\phi_c = 0.40$; (B) $R_g/R = 0.078$, $\phi_c = 0.40$ and (C) $R_g/R = 0.053$, $\phi_c = 0.45$. Full lines are linear least squares fits for $qD < 0.7$. The extracted values of heterogeneity correlation length and $q = 0$ amplitude are listed.

Thus, we adopt the simplest Gaussian fractal model for which the mean square radius of gyration is [75–77]

$$R_g^2 = \frac{N^{2\nu} D^2}{(2\nu + 1)(2\nu + 2)}. \tag{7}$$

Here D is the particle diameter, N is the number of particles in a cluster and $1/\nu = d_f$ is the fractal dimension. The corresponding cluster diameter is $\xi_c = 2R_g$, where R_g is now the cluster radius of gyration. The standard idea [78] for non-interpenetrating, monodisperse clusters is that they grow until the cluster volume fraction reaches a maximum jamming value, ϕ_{MAX}. This condition then yields

$$\xi_c/D = 2(\phi_{MAX}/8\phi_c)^{\nu/(3\nu-1)}[(1+2\nu)(2+2\nu)]^{1/2(3\nu-1)}. \tag{8}$$

For our experimental systems, $\phi_c \sim 0.4$. Based on a random close packing value of $\phi_{MAX} = 0.64$, equation (7) yields $\xi_c/D \sim 2.1$, 2.4, 2.4 and 3.2 for fractal dimensions of 1.75 (DLCA), 2 (chains or polydisperse ensemble of percolated clusters), 2.1 (RLCA) and 2.3, respectively. Fractal dimensions corresponding to classic kinetic aggregation and static percolation models are indicated in parentheses [78]. For relatively low volume fraction depletion-induced gels, typical values for the fractal dimension are ∼2.0–2.2, which would correspond to calculated cluster sizes of ∼2–3 particle diameters for our $\phi_c = 0.4$ system. Experimentally, one sees from figures 3 and 12 that there are no fractal signatures in $S(q)$ on these relatively small length scales. This reinforces our argument given in section 4.2 that fractal geometry is not relevant at the high particle volume fractions of present interest.

7. Summary

A systematic experimental study of polymer-induced changes of collective colloid structure in the fluid and gel states has been carried out using USAXS. The focus was on small polymer depletants where a transition from the homogeneous fluid phase to a nonequilibrium gel state occurs with increasing polymer additions. As the polymer concentration is increased, we find:

(i) the low angle concentration fluctuations monotonically increase in the fluid phase as expected,
(ii) the characteristic length scale of the local cage decreases and tends to saturate, and
(iii) the intensity of the wide angle cage order peak varies in a non-monotonic manner, first decreasing and then increasing as the gel boundary is approached.

These equilibrium structural changes depend in a systematic fashion on the colloid volume fraction, the polymer–colloid size asymmetry and solvent quality [28], in a manner which is in near-quantitative agreement with the no adjustable parameter PRISM theory calculations.

By combining the accurate equilibrium theory with experimental observations, the loss of ergodicity and nonequilibrium structure formation in the gel state can be deduced. Abrupt departures between theory and experiment on the ∼2–3 particle diameter and greater length scales are observed as the gel boundary is traversed. Hence, USAXS measurements in conjunction with theory is a novel tool for both locating the gelation transition and quantifying the deviations of gel structure from equilibrium behaviour.

By combining the results of all the scattering experiments and theoretical calculations a qualitative picture of the gel structure has been constructed as indicated in figure 11. For $qD < 10$, corresponding to length scales on the order of a particle diameter and larger, all structural features in the gel are (nearly) independent of polymer concentration, indicating a freezing of correlations. On the local cage scale, gelation results in particle localization and a freezing in of liquid-like collective packing. On intermediate $\xi_c \sim 3$ particle diameter length scales, concentration fluctuations are suppressed by a significant factor of ∼3 relative to equilibrium fluid and theoretical expectations. This suggests that a local densification or compaction process is triggered in the gel, resulting in reduced compressibility and the formation of small ‘clusters’. The latter are likely polydisperse, percolated, and

interpenetrating to some extent. The compressibility suppression/local densification makes sense mechanically, given the stiff nature of the gel, and the generic connection between osmotic concentration fluctuations and a compressive modulus or yield stress [79, 80]. In reality the local density change may be quite small since it is driven by depletion attractions with a spatial range $\sim R_g \sim$ 3–5 nm $\ll R \sim$ 59 nm. A 'pseudo plateau' in $S(q)$ is also present on the $qD \sim$ 2–3 scale, with an absolute magnitude that is consistent with real space confocal measurements of concentration fluctuations on finite length scales in dense particle gels [30].

Gelation also results in the emergence of large amplitude scattering at low wavevectors. The power law 'low angle upturn' begins at a length scale of $\sim$4–6D and follows a Porod-like scaling. The fact that the gel forms directly from the homogeneous fluid phase, and the near-independence of the low angle upturn feature to variations in polymer concentration and size asymmetry, strongly suggests it is not associated with metastable equilibrium phase separation boundaries. Rather, its origin is likely a consequence of the smaller scale process of cluster formation and compaction, and the attendant creation of meandering internal interfaces, small-scale voids and/or heterogeneities required by global mass conservation.

Analysis of the low angle scattering patterns using the Debye–Bueche random two-phase model yields sensible values for the amplitude of the quenched disorder concentration fluctuations and a heterogeneity length scale of $\xi_v \sim$ 5–8D. The latter value seems consistent with experimental estimates of a cluster size of $\xi_c \sim 4$ particle diameters based on the 'breaking away' of the low angle scattering data from a Porod-like law. Whether the low angle scattering is best interpreted as indicating sharp interfaces between dense clusters with diffuse fractal surfaces, or some other microscopic model, cannot be uniquely established.

Non-fractal, Porod-like scattering has been previously observed in polymer–colloid mixtures [6], thermoreversible adhesive hard-sphere suspensions [81] and silica colloids in a water–lutidine mixture [82]. The polymer–colloid study is most relevant to our work and there are some similarities but also multiple strong differences. Verhaegh *et al* [6] used light scattering to study a relatively low volume fraction ($\phi_c \sim 0.1$) polymer–colloid mixture with a size symmetry ratio of $R_g/R = 0.25$, which is much larger than our mixtures where $R_g/R \sim$ 0.05–0.08. This difference has very important consequences since for the longer range depletion attraction system gelation occurs in a fluid–fluid two-phase region. Hence, the nonequilibrium gelation process is strongly coupled to, and triggered by, spinodal phase separation where a bicontinuous two-phase structure exist. This is in strong contrast to our system where gelation proceeds directly from the homogeneous phase [3, 5]. Moreover, in the two-phase region gelation is believed to be induced by the thermodynamically driven densification of colloids in the particle-rich phase. A low angle scattering peak and non-fractal Porod-like behaviour at wavevectors above the peak, characteristic signatures of a spinodal decomposing mixture, are observed [6]. The Porod behaviour is interpreted in the classic manner as due to sharp interfaces between the dense and dilute colloid phases. The low angle peak occurred on a length scale of $\sim$100 particle diameters, which significantly exceeds what can be probed via x-ray scattering in our system. Gravity-driven settling was also observed [6], in contrast to our much higher volume fraction suspensions which do not settle on any reasonable timescale. We also note that dense, non-fractal, reversible aggregation of low volume fraction charged silica and polystyrene colloidal suspensions has been observed in the one-phase region [82, 83]. Porod scattering is seen but no small angle peaks are evident. The mechanism of particle attraction and aggregation in these systems is not well understood.

We expect there are strong rheological consequences of the heterogeneous gel structure. Buscall *et al* [80] have suggested that the ratio of the shear G and bulk K modulus is a

constant, dependent on Poisson's ratio ν through the relation $K/G = 2(1+\nu)/3(1-2\nu)$. At the gelation transition we find a drop (compared to equilibrium predictions) in the compressibility $S(qD \sim 2\text{–}3)$ at intermediate length scales. The bulk modulus is given by $K = -(V)\,\mathrm{d}P/\mathrm{d}V = kT\rho/S(0)$. Hence reduced compressibilities at the cluster length scale are consistent with an increase in the modulus and compressive yield stress of the suspension at the gel transition. From figure 10, we estimate a bulk modulus of ∼10–20 Pa, which is consistent within an order of magnitude of the elastic shear modulus determined from rheological measurements [84]. The extent to which the dynamic modulus can be deduced from the intensity of the intermediate scale structure factor, especially its detailed dependence on polymer concentration, solvent quality, volume fraction and size asymmetry, is not clear and requires further study. The overlap between the quenched disorder low angle scattering and the intermediate scale scattering contributions presents difficulties in any quantitative analysis and correlation of osmotic and mechanical properties in gels.

A related issue is that the large concentration fluctuations in the low angle upturn region correspond to an (extracted) $S_{D-B}(0)$ which is several orders of magnitude larger than $S(qD \sim 2\text{–}3)$. These low angle fluctuations do not seem to have mechanical consequences, since they would lead to compressive and shear moduli far smaller than observed [79, 84]. Indeed, in crosslinked polymer gels [72] and ionomers [71] there is also a quenched heterogeneous structure resulting in a sharp upturn of $S(q)$ at low q. For these materials, it is believed that such excess low angle scattering is not important in determining bulk mechanical properties.

Finally, there is the issue of connections between gel structure, stress transmission and bulk mechanical properties. On the particle length scale and longer, $S(q)$ is nearly independent of polymer concentration and size asymmetry in the gel. On the other hand, mechanical properties such as the shear elastic modulus do depend significantly on the latter control variables [8, 29, 63, 65, 79, 80, 84]. These facts are consistent with the ideas of idealized MCT of gelation due to short-range attractive interactions [19, 20, 22, 38, 62]. MCT argues (especially at high volume fractions) that physical bonds between colloids trigger gelation, and particle localization occurs on length scales controlled by the range of the depletion attraction which determines the mechanical properties. However, MCT also assumes that structural correlations on the depletion range length scale remain in equilibrium. Although plausible, scattering experiments cannot directly test this idea since $R_g \ll R$. However, theoretical studies which combine MCT with PRISM theory for the required structural information can provide an insight into this question. These and related issues will be explored experimentally and theoretically in future publications.

Acknowledgments

The authors would like to thank P R Jemian and J Ilavsky for advice and support in gathering USAXS data at the synchrotron facility at Argonne National Laboratory. The UNICAT facility at the APS is supported by the University of Illinois at Urbana-Champaign, Materials Research Laboratory (US DOE, the State of Illinois-IBHE-HECA and the NSF), Oak Ridge National Laboratory (US DOE under contract with UT-Battelle LLC), National Institute of Standards and Technology (US Department of Commerce) and UOP LLC. The APS is supported by the US DOE, Basic Energy Sciences, Office of Science under contract no W-31-109-ENG-38. We gratefully acknowledge Dr Matthias Fuchs for many discussions and prior collaborations. This work was supported by the Nanoscale Science and Engineering Initiative of the National Science Foundation under NSF Award Number DMR-0117792.

References

[1] Russel W B, Saville D A and Schowalter W R 1989 *Colloidal Dispersions* (Cambridge: Cambridge University Press)
[2] Poon W C K 2002 *J. Phys.: Condens. Matter* **14** R859
[3] Ramakrishnan S, Fuchs M, Schweizer K S and Zukoski C F 2002 *J. Chem. Phys.* **116** 2201
[4] Ramakrishnan S, Fuchs M, Schweizer K S and Zukoski C F 2002 *Langmuir* **18** 1082
[5] Shah S A, Chen Y L, Schweizer K S and Zukoski C F 2003 *J. Chem. Phys.* **118** 3350
[6] Verhaegh N A M, Asnaghi D, Lekkerkerker H N W, Giglio M and Cipelletti L 1997 *Physica* A **242** 104
[7] Patel P D and Russel W B 1989 *J. Colloid Interface Sci.* **131** 201
[8] Buscall R, McGowan I J and Mumme-Young C A 1990 *Faraday Discuss. Chem. Soc.* **90** 115
[9] Kulkarni A M, Dixit N M and Zukoski C F 2003 *Faraday Discuss.* **123** 37
[10] Asakura S and Oosawa F 1954 *J. Chem. Phys.* **22** 1255
[11] Asakura S and Oosawa F 1958 *J. Polym. Sci.* **33** 183
[12] Anderson V J and Lekkerkerker H N W 2002 *Nature* **416** 811
[13] Gast A P, Hall C K and Russel W B 1983 *J. Colloid Interface Sci.* **96** 251
[14] Ilett S M, Orrock A, Poon W C K and Pusey P N 1995 *Phys. Rev.* E **51** 1344
[15] Vrij A 1978 *J. Chem. Phys.* **69** 1742
[16] van Megen W and Underwood S M 1994 *Phys. Rev.* E **49** 4206
[17] Gotze W 1999 *J. Phys.: Condens. Matter* **11** A1
[18] Gotze W and Sjogren L 1992 *Rep. Prog. Phys.* **55** 241
[19] Bergenholtz J, Fuchs M and Voigtmann Th 2000 *J. Phys.: Condens. Matter* **12** 6575
[20] Dawson K, Foffi G, Fuchs M, Gotze W, Sciortino F, Sperl M, Tartaglia P, Voigtmann Th and Zaccarelli E 2001 *Phys. Rev.* E **63** 011401
[21] Eckert T and Bartsch E 2002 *Phys. Rev. Lett.* **89** 125701
[22] Pham K N, Puertas A M, Bergenholtz J, Egelhaaf S U, Moussaid A, Pusey P N, Schofield A B, Cates M E, Fuchs M and Poon W C K 2002 *Science* **296** 104
[23] Fabbian L, Gotze W, Sciortino F, Tartaglia P and Thiery F 1999 *Phys. Rev.* E **59** R1347
[24] Ye X, Narayanan T, Huang J S and Tong P 1996 *Phys. Rev. Lett.* **76** 4640
[25] Moussaid A, Poon W C K, Pusey P N and Soliva M F 1999 *Phys. Rev. Lett.* **82** 225
[26] Fuchs M and Schweizer K S 2002 *J. Phys.: Condens. Matter* **14** R239
[27] Lekkerkerker H N W, Poon W C K, Pusey P N, Stroobants A and Warren P B 1992 *Europhys. Lett.* **20** 559
[28] Shah S A, Ramakrishnan S, Chen Y L, Schweizer K S and Zukoski C F 2003 *Langmuir* at press
[29] Dinsmore A D and Weitz D A 2002 *J. Phys.: Condens. Matter* **14** 7581
[30] Varadan P and Solomon M J 2003 *Langmuir* **19** 509
[31] Stober W, Fink A and Bohn E 1968 *J. Colloid Interface Sci.* **26** 62
[32] Bogush G H, Tracy M A and Zukoski C F 1988 *J. Non-Cryst. Solids* **104** 95
[33] van Helden A K, Jansen J W and Vrij A 1981 *J. Colloid Interface Sci.* **81** 354
[34] Carnahan N F and Starling K E 1970 *J. Chem. Phys.* **53** 600
[35] Hansen J P and McDonald I R 1986 *Theory of Simple Liquids* 2nd edn (New York: Academic)
[36] de Gennes P G 1979 *Scaling Concepts in Polymer Physics* (Ithaca, NY: Cornell University Press)
[37] Berry G C 1966 *J. Chem. Phys.* **44** 4550
[38] Bergenholtz J, Poon W C K and Fuchs M 2003 *Langmuir* **19** 4493
[39] Solomon M J and Varadan P 2001 *Phys. Rev.* E **63** 051402
[40] Rueb C J and Zukoski C F 1997 *J. Rheol.* **41** 197
[41] Ilavsky J, Allen A J, Long G G and Jemian P R 2002 *Rev. Sci. Instrum.* **73** 1660
[42] Horner K D, Topper M and Ballauff M 1997 *Langmuir* **13** 551
[43] Glatter O and Kratky O 1982 *Small-Angle X-Ray Scattering* (New York: Academic)
[44] Chandler D 1982 *Studies in Statistical Mechanics* (Amsterdam: North-Holland) p 274
[45] Schweizer K S and Curro J G 1994 *Adv. Polym. Sci.* **116** 319
[46] Schweizer K S and Curro J G 1997 *Adv. Chem. Phys.* **98** 1 and references therein
[47] Chandler D and Andersen H C 1972 *J. Chem. Phys.* **57** 1930
[48] Fuchs M and Schweizer K S 2000 *Europhys. Lett.* **51** 621
[49] Fuchs M and Schweizer K S 2001 *Phys. Rev.* E **64** 021514
[50] Chen Y L, Schweizer K S and Fuchs M 2003 *J. Chem. Phys.* **118** 3880
[51] Percus J K and Yevick G J 1958 *Phys. Rev.* **110** 1
[52] Schmidt M, Lowen H, Brader J M and Evans R 2000 *Phys. Rev. Lett.* **85** 1934
[53] Schmidt M and Fuchs M 2002 *J. Chem. Phys.* **117** 6308

[54] Sear R P 2001 *Phys. Rev. Lett.* **86** 4696
[55] Tuinier R, Vliegenthart G A and Lekkerkerker H N W 2000 *J. Chem. Phys.* **113** 10768
[56] Poon W C K, Starrs L, Meeker S P, Moussaid A, Evans R M L, Pusey P N and Robins M M 1999 *Faraday Discuss.* **112** 143
[57] Poon W C K, Pirie A D, Haw M D and Pusey P N 1997 *Physica* A **235** 110
[58] Poon W C K, Pirie A D and Pusey P N 1995 *Faraday Discuss.* **101** 65
[59] Poon W C K, Selfe J S, Robertson M B, Ilett S M, Pirie A D and Pusey P N 1993 *J. Physique* II **3** 1075
[60] Goodwin J W, Hughes R W, Kwaambwa H M and Reynolds P A 2000 *Colloids Surf.* A **161** 339
[61] Patel P D and Russel W B 1987 *J. Rheol.* **31** 599
[62] Bergenholtz J and Fuchs M 1999 *Phys. Rev.* E **59** 5706
[63] Shih W-H, Shih W Y, Kim S, Liu J and Aksay I A 1990 *Phys. Rev.* A **42** 4772
[64] Martin J E and Hurd A J 1987 *J. Appl. Cryst.* **20** 61
[65] Segre P N, Prasad V, Schofield A B and Weitz D A 2001 *Phys. Rev. Lett.* **86** 6042
[66] Ferri F, Frisken B J and Cannell D S 1991 *Phys. Rev. Lett.* **67** 3626
[67] Varadan P and Soloman M J 2001 *Langmuir* **17** 2918
[68] McCarthy D W, Mark J E and Schaefer D W 1998 *J. Polym. Sci. Polym. Phys.* **36** 1167
[69] Zhou J and Sheng J 1997 *Polymer* **38** 3727
[70] Kalhoro M S, Gabrys B J, Zajac W, King S M and Peiffer D G 2001 *Polymer* **42** 1679
[71] Wu D Q, Chu B, Lundberg R D and MacKnight W J 1993 *Macromolecules* **26** 1000
[72] Benguigui L and Boue F 1999 *Eur. Phys. J.* B **11** 439
[73] Pogodina N V, Siddiquee S K, van Egmond J W and Winter H H 1999 *Macromolecules* **32** 1167
[74] Debye P and Bueche A M 1949 *J. Appl. Phys.* **120** 518
[75] Cates M E 1984 *Phys. Rev. Lett.* **53** 926
[76] Muthukumar M 1985 *J. Chem. Phys.* **83** 3161
[77] Fuchs M and Schweizer K S 1997 *J. Chem. Phys.* **106** 347
[78] Vicsek T 1989 *Fractal Growth Phenomenon* (Singapore: World Scientific)
[79] Buscall R, McGowan I J, Mills P D A, Stewart R F, Sutton D, White L R and Yates G E 1987 *J. Non-Newton. Fluid Mech.* **24** 183
[80] Buscall R, Mills P D A, Goodwin J W and Larson D W 1988 *J. Chem. Soc. Faraday Trans.* **84** 4249
[81] Verduin H and Dhont J K G 1995 *J. Colloid Interface Sci.* **172** 425
[82] Broide M L, Garrabos Y and Beysens D 1993 *Phys. Rev.* E **47** 3768
[83] Gallagher P D, Kurnaz M L and Maher J V 1992 *Phys. Rev.* A **46** 7750
[84] Shah S A, Chen Y L, Schweizer K S and Zukoski C F 2003 *J. Chem. Phys.* submitted